SIMULATION OF DEFLAGRATION-TO-DETONATION TRANSITION OF LEAN H2-CO-AIR MIXTURES IN OBSTRUCTED CHANNELS

Barfuss, C.[1], Heilbronn, D.[1] and Sattelmayer, T.[1]
[1] Technical University of Munich (TUM), Chair of Thermodynamics, Boltzmannstraße 15, Garching, 85747, Germany
***Email: barfuss@td.mw.tum.de**

ABSTRACT

The possibility of flame acceleration (FA) and deflagration-to-detonation transition (DDT) when homogeneous hydrogen-carbon monoxide-air (H_2-CO-air) mixtures are used rises the need for an efficient simulation approach for safety assessment. In this study a modelling approach for H_2-CO-air flames, incorporating deflagration and detonation within one framework, is presented. It extends the previous work on H_2-air mixtures. The deflagration is simulated by means of the turbulent flame speed closure model incorporating a quenching term. Since high flow velocities, e.g. the characteristic speed of sound of the combustion products, are reached during FA, the flow passing obstacles generates turbulence at high enough levels to partially quench the flame. Partial flame quenching has the potential to stall the onset of detonation. An altered formulation for quenching is introduced to the modelling approach to better account for the combustion characteristics for accelerating lean H_2-CO-air flames. The presented numerical approach is validated with experimental flame velocity data of the small-scale GraVent test rig [1] with homogeneous fuel contents of 22.5 and 25.0 vol-% and fuel compositions of 75/25 and 50/50 vol-% H_2/CO, respectively. The impact of the quenching term is further discussed on simulations of the FZK-7.2m test rig [2] whose obstacle spacing is smaller than the spacing in the GraVent test rig.

Keywords: *CFD, DDT, hydrogen-carbon monoxide, obstructed channel, quenching*

NOMENCLATURE

Latin Characters

a	Thermal diffusivity
a_{pr}	Speed of sound of products
c	Reaction progress variable
D	Diffusion coefficient
D_{CJ}	Chapman-Jouguet velocity
g	Velocity gradient
G	Quenching factor
p	Pressure
S_{L}	Laminar flame speed
t	Time
T	Temperature
x	Mole fraction
x_j	Cartesian coordinate

Greek Characters

ρ	Density
$\dot{\omega}$	Source term
τ	Dimensionless ignition delay time
Ξ	Flame wrinkling factor
ϕ	Equivalence ratio
ε	Dissipation rate of turbulent energy
ν	Kinematic viscosity
σ	Standard deviation

Subscripts

eff	Effective
def	Deflagrative
vol	Volumetric
comp	Computational
ign	Self-ignition
u	Unburned
0	Reference conditions
cr	Critical
F	Fuel
H2	Hydrogen

1.0 MOTIVATION

The intended or unintended presence of hydrogen (H_2)-carbon monoxide (CO) mixtures in technical applications rises the need of a safety evaluation when combustible mixtures with air are formed. For

instance, in a severe accident scenario of a nuclear power plant involving molten-core-concrete-interaction (MCCI), H_2 and CO are formed in large amounts. Mixed with ambient air, the fuel-oxidizer mixture is capable to ignite, accelerate and eventually transition into a detonation, as the Fukushima-Daichii accident has shown [3]. The high dynamic pressure loads on the confining structure have severe consequences for personnel, equipment and infrastructure. Syngas (H_2-CO) finds further application as reactant for many processes in the chemical industry as well as fuel in the energy sector [4,5]. Due to the versatility of possible accident scenarios, an efficient simulation approach for flame acceleration (FA) and deflagration-to-detonation transitions (DDT) is required.

In order to account for the complex structure of various technical applications, a CFD solver based on the OpenFOAM framework, which supports unstructured meshes, is developed. The numerical approach is computed on under-resolved meshes to increase the efficiency. Thus, most physical effects have to be modelled. Deflagration and the successive transition into a detonation is calculated within one solver. It is build up on previous developments by [6,7]. The previous achievements involve the applicability of the solver on large-scale accident scenarios. The main goal of the solver development is the correct prediction of flame tip velocities and the according pressure loads on confining structures.

The current work extends the combustible homogeneous H_2-air mixtures by CO. Necessary additions of several flame characteristics, e.g. laminar flame speeds, have been presented before [8]. In the current study, the CO extension is validated against flame velocity data of small-scale experiments in the GraVent test rig. On small dimensions, the effect of partial flame quenching behind obstacles shows greater influence on the flame acceleration than on large-scale. Thus, an elaborated treatment of the turbulent flame speed closure (TFC) model's quenching term is required in order to accurately predict the experimental results. The impact of the quenching term in small-scale applications is further discussed on the flame velocity data from the FZK-7.2m geometry which has a smaller spacing between obstacles.

2.0 MODELLING APPROACH

After a general description of the solver, the TFC model [9] and the quenching term in particular are discussed. One dimensional counter-flow flame simulations using Cantera [10] are used to estimate critical velocity gradients for flame extinction in the quenching term. In order to evaluate quenching characteristics during FA, a correlation for H_2-CO fuels including a pressure dependency is presented.

2.1 Solver

In this work a CFD solver based on the open-source CFD libraries OpenFOAM is used. Because the investigated phenomenon of DDT is a transient problem with a mixed parabolic-hyperbolic nature, the Favre-averaged unsteady compressible Navier-Stokes equations are solved. The ideal gas law and a transport equation for the internal total energy complete the governing equations. The deflagrative flame acceleration is driven by turbulent combustion. Thus, turbulence is considered by the well-established k-ω SST turbulence model with wall functions as boundary conditions [11]. The onset of detonation is eventually triggered by shock-focusing or by preconditioning of the fresh gas through pressure waves [12]. In order to preserve the pressure waves, the simulation is build up on an explicit and density-based architecture. The convective terms are modelled with an approximated Riemann solver, namely the Harten-Lax-van Leer-Contact (HLLC) scheme [13]. An adaptive time step size defined by an acoustic Courant-Friedrichs-Lewy criterion (flow velocity + speed of sound) of 0.3 is applied. Due to the main interest in the flame trajectory and the build-up of the dynamic pressure loads during an accident scenario, the simulations can be computed on an under-resolved meshes. In order to maintain a sufficient resolution in relevant domain sections adaptive mesh refinement (AMR) is used. Relevant domain sections are the vicinity of the flame, regions of strong shocks and regions of high turbulence production. The AMR method includes an unrefinement mechanism decreasing the number of cells once the flame has passed.

2.2 Flame propagation

The applicability of the solver on large-scale accidents scenarios was enabled by the implementation of a geometrical volume of fluid method [14]. Despite the under-resolved mesh, the flame front can be resolved with several cells in the small-scale scenarios, which is in contrast to the implementation of the volume of fluid method. The treatment of the flame front as discrete interface in the volume of fluid method leads to a strong grid dependency on the small-scale scenarios. Thus, the transport equation of the reaction progress variable c

$$\frac{\partial}{\partial t}(\bar{\rho}\tilde{c}) + \frac{\partial}{\partial x_j}(\bar{\rho}\tilde{c}\tilde{u}_j) - \frac{\partial}{\partial x_j}\left(\bar{\rho}D_{\mathrm{eff}}\frac{\partial \tilde{c}}{\partial x_j}\right) = \max(\dot{\omega}_{\mathrm{def}}; \dot{\omega}_{\mathrm{vol}}) \tag{1}$$

is used for flame propagation in small-scale scenarios. ρ is the density, u the velocity, D_{eff} the effective diffusion coefficient. The application of a reaction progress variable highly benefits the computational efficiency in comparison to an individual transport equation for each specie. The reaction progress variable is unity in the burned state and zero in the unburned. The burned gas composition is precalculated and provided to the solver as interpolation table depending on fuel content, temperature and pressure. The equation is closed by the maximum out of the deflagrative source term $\dot{\omega}_{\mathrm{def}}$ and the volumetric source term $\dot{\omega}_{\mathrm{vol}}$. The volumetric source term accounts for the self-ignition of the fresh gas. It is triggered when the ratio of the computational time and the ignition delay time $\tau = t_{\mathrm{comp}}/t_{\mathrm{ign}}$ becomes unity. The ignition delay times for H_2-CO fuels are precalculated in the chemical kinetic solver software Cantera [10] using the mechanism of Li [15]. The ignition delay times are provided to the solver by interpolation tables over a range of temperatures, pressures and fuel compositions. For further explanation, the reader is referred to the previous work of [14].

The deflagrative source term describes the flame acceleration and preconditions the fresh gas for self-ignition at later stages. The acceleration process will eventually lead to pressure waves triggering self-ignition of the fresh gas and thus initiating DDT. The turbulent flame speed closure (TFC) model of equation 2 is used.

$$\dot{\omega}_{\mathrm{def}} = \overline{\rho}_{\mathrm{u}} G \Xi S_{\mathrm{L}} \left|\frac{\partial \tilde{c}}{\partial x_j}\right| \tag{2}$$

Ξ represents the flame wrinkling factor and S_{L} the laminar flame speed. The turbulent flame speed is described by the product of wrinkled flame surface and laminar flame speed. A transport equation is solved for the flame wrinkling factor representing the evolution of flame front wrinkling of the turbulent flame. The transport equation tends towards an equilibrium value determined by the Dinkelacker ansatz [16]. The formulation includes the effect of thermo-diffusive instabilities by an effective Lewis-number as well as the pressure effect on flame wrinkling. The fuel addition of CO in the model was previously presented in [8].

The laminar flame speed is correlated at the reference conditions of T_0=298 K and p_0=1.013 bar. They are derived from 1D free flame simulations in Cantera using the Davis reaction mechanism [17]. Since the laminar flame speed and the ignition delay times are provided to the solver as precalculated or correlated values, the most suitable reaction mechanisms can be used. The decision for each parameter is based on the comparison [18]. The correlation relates the laminar flame speed with the equivalence ratio ϕ and the volume fraction of hydrogen in the fuel $x_{\mathrm{H2,F}}$. The pressure and the temperature dependency is described by a power law. The correlation as well as the power law exponents have been presented in [8]. Recently, laminar flame speed measurements on spherical outward propagating flames have been conducted by ProScience GmbH [19]. The data of H_2-CO fuels ranges from the flammability limits across $\phi = 1$ with varying fuel compositions of H_2 and CO. Figure 1 shows a comparison of the laminar flame speed data above 20 vol-% of fuel. The measurements have not been corrected for the effects of instabilities and flame stretch. This causes higher measured flame speeds for hydrogen rich mixtures in comparison to literature values [19]. The correlation sufficiently matches the experiment, with better results for low amounts of hydrogen in the fuel.

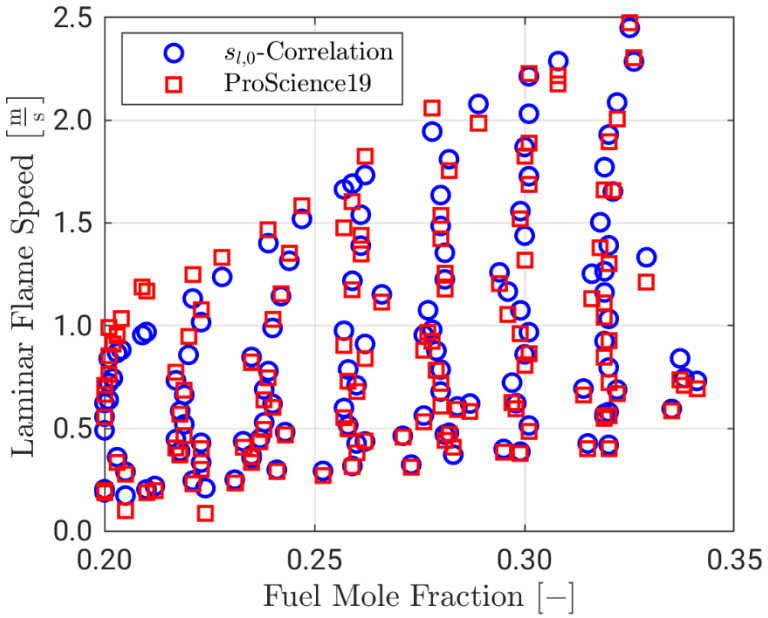

Figure 1. Comparison of measured and correlated laminar flame speed data at reference conditions

All gas properties used in the deflagration source term are in respect of the unburned state. This requires additional correlation of the unburned gas properties and an unburned temperature. The unburned temperature and unburned density is estimated by isentropic relations in respect of the pressure in order to omit the temperature rise due to the flame. For the most part of the FA the underlying assumption of an isobaric combustion is valid.

2.3 Flame Quenching

The deflagration source term utilises a quenching term factoring in the possibility of flame quenching at very high turbulence [9]. The relation is derived from the log-normal distribution of the turbulent dissipation rate ε. The following error function is used to estimate the quenching term G:

$$G = \frac{1}{2}\operatorname{erfc}\left\{-\frac{1}{\sqrt{2}\sigma}\left(\ln\left(\frac{\varepsilon_{\mathrm{cr}}}{\varepsilon}\right)+\frac{\sigma}{2}\right)\right\} \tag{3}$$

In equation 3, σ is the standard deviation of the log-normal distribution. σ is calculated from the ratio of the turbulent and the Kolmogorov length scale as $\sigma = 0.26\ln\left(l_{\mathrm{t}}/l_{\eta}\right)$. Equation 3 utilises a critical dissipation rate $\varepsilon_{\mathrm{cr}}$ in order to check whether quenching occurs. The critical dissipation rate is described as follows.

$$\varepsilon_{\mathrm{cr}} = 15\nu g_{\mathrm{cr}}^2 \tag{4}$$

$\varepsilon_{\mathrm{cr}}$ is estimated from the kinematic viscosity ν and the critical velocity gradient g_{cr}, which relates to the flame stretch required to quench a flame. The authors of the TFC model derived the relation of the critical velocity gradient in equation 5 from dimension analysis [20]. They state, that the velocity gradient should be treated as a tuning factor. For all previous investigations the expression of equation 5 has been used in the modelling approach. a corresponds to the thermal diffusivity.

$$g_{\mathrm{cr}} = \frac{S_{\mathrm{L}}^2}{a} \tag{5}$$

In CO containing fuels, the laminar flame speed decreases as figure 1 indicates. Thus, the critical velocity gradient evaluated by equation 5 would decrease as well. Since similar velocities have to be reached for a DDT in H_2-CO fuels, partial quenching becomes more likely for CO containing fuels

according to equation 5. But even at fuel compositions of 25 vol-% H_2 in a H_2-CO fuel mixture, combustion characteristics of the mixture, like the Lewis number, is dominated by hydrogen [8,21]. The flame speed of fuels with a Lewis numbers less than unity increases in the presence of flame stretching, which will consequently lead to a higher critical velocity gradient for flame extinction [22].

The critical velocity gradient can be determined from 1D simulations of premixed counter-flow flames in Cantera with the reaction mechanism of David [18]. Heat losses are neglected, because the residence time of the flame is very short for fast flames. g_{cr} is obtained by gradually increasing the flame stretch until the flame extinguishes. A fresh-to-burned configuration is applied. Hence, the flame is considered extinct, when the threshold of 1.25 times the equilibrium concentration of OH-radicals was nowhere to be found in the computational domain.

Figure 2 shows a comparison of g_{cr} from the 1D simulations with corresponding values from equation 5. The g_{cr} strongly deviate for lean fuel-air mixtures. Values from the 1D simulations are higher by roughly one order of magnitude. The dominance by hydrogen over the combustion characteristics can be seen in the fact, that the 1D results of pure H_2 as fuel ($x_{\mathrm{H2,F}} = 1.0$) and the results of the 50/50 vol-% H_2/CO fuel mixture ($x_{\mathrm{H2,F}} = 0.5$) deviate less from each other than the ones evaluated by equation 5. It should be mentioned that the velocity gradient or flame stretch in laminar steady state flows differs from the more complex flame stretch by turbulent three-dimensional vortices, which alter with time. g_{cr} can be even higher in a turbulent flow, because not the entire spectrum of turbulent eddies contributes to flame stretch [23].

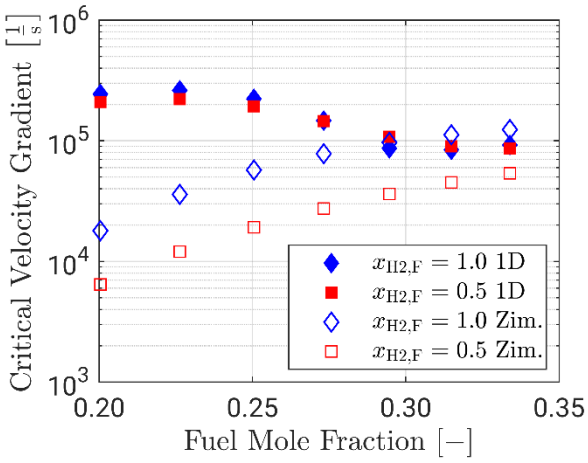

Figure 2. g_{cr} at reference conditions evaluated by 1D simulations and equation 5

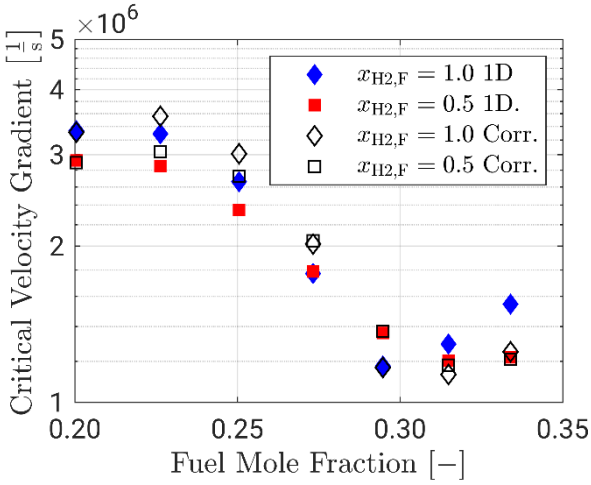

Figure 3. Comparison of correlated g_{cr} at 10 bar with 50 and 100 vol-%

g_{cr} values determined from 1D simulations have been successfully used in the TFC model for steady state combustion [24]. But in the transient FA of lean H_2-CO-air mixtures significantly higher critical velocity gradients will occur due to the continuous pressure rise [22]. Thus, a correlation for runtime evaluation of g_{cr} is derived from a set of g_{cr} values based on 1D simulations. The mixtures composition varies with equivalence ratios between 0.6 and 1.5 and hydrogen contents in the fuel $x_{\mathrm{H2,F}}$ between 1.0 and 0.25. All mixture compositions are evaluated at pressures from 1 to 10 bar. In accordance with the modelling approach the artificial unburned temperature was adjusted to the pressure rise in respect of isentropic relations.

Equation 6 is used to evaluate critical velocity gradients in H_2-CO-air mixtures. The fuel composition is considered by multiplying the ratio factor $R_{x_{\mathrm{H2,F}}}$ onto the critical velocity gradient of hydrogen at reference conditions $g_{\mathrm{cr,H2,0}}$.

$$g_{\mathrm{cr}} = g_{\mathrm{cr,H2,0}}\, R_{x_{\mathrm{H2,F}}} \left(\frac{P}{P_0}\right)^n \tag{6}$$

The equation uses a polynomial for $g_{\mathrm{cr,H2,0}}$ as well as a two-dimensional polynomial for the ratio factor $R_{x_{\mathrm{H2,F}}}$. The pressure dependency is considered by a power law with the exponent n. The polynomial of $g_{\mathrm{cr,H2,0}}$ is of the fourth order and is evaluated separately for fuel contents above and below $\phi = 1$. The coefficients of the polynomial are presented in table 1 for fuel contents above and below $\phi = 1$.

$$g_{\mathrm{cr,H2,0}} = \left(C_5 x_{\mathrm{F}}^4 + C_4 x_{\mathrm{F}}^3 + C_3 x_{\mathrm{F}}^2 + C_2 x_{\mathrm{F}} + C_1\right) \cdot 10^9 \tag{7}$$

Table 1. Constants of the critical velocity gradient polynomial of H_2-air mixtures

	C_5	C_4	C_3	C_2	C_1
$\phi \leq 1$	3.0538	-2.7546	0.89512	-0.12397	$6.3444 \cdot 10^{-3}$
$\phi > 1$	3.3272	-4.6170	2.3929	-0.54882	$4.7074 \cdot 10^{-2}$

The two-dimensional polynomial of the ratio factor is also evaluated separately for overall fuel contents to either side of a stoichiometric mixture. The coefficients of the polynomial are stated in table 2.

$$R_{x_{\mathrm{H2,F}}} = C_{00} + C_{10} x_{\mathrm{F}} + C_{01} x_{\mathrm{H2,F}} + C_{20} x_{\mathrm{F}}^2 + C_{11} x_{\mathrm{F}} x_{\mathrm{H2,F}} + C_{02} x_{\mathrm{H2,F}}^2 + C_{21} x_{\mathrm{F}}^2 + \cdots$$
$$\cdots + C_{12} x_{\mathrm{F}} x_{\mathrm{H2,F}}^2 + C_{03} x_{\mathrm{H2,F}}^3 \tag{8}$$

Table 2. Constants of the ratio factor polynomial factoring in the fuel composition of H_2-CO fuels

	C_{00}	C_{10}	C_{01}	C_{20}
$\phi \leq 1$	5.9988	-50.3875	-4.3169	109.4983
$\phi > 1$	11.2312	-62.8908	-3.8542	92.9382

	C_{11}	C_{02}	C_{21}	C_{12}	C_{03}
$\phi \leq 1$	52.4679	-1.2152	-103.3405	-5.163	0.9123
$\phi > 1$	41.4103	-5.3054	-75.4774	9.6767	0.9064

A mean pressure exponent of $n = 1.14$ for all mixture compositions has been deducted from the 1D simulation results. Figure 3 shows the comparison of correlated g_{cr} and 1D simulation of g_{cr} at the elevated pressure of 10 bar. The pressure exponent deviates more intensely from the mean value for fuel compositions with greater amounts of H_2. Thus, better agreement can be shown for the fuel composition of $x_{\mathrm{H2,F}} = 0.5$. Suitable agreement can be achieved for all fuel compositions in lean fuel-air mixtures, which are the most relevant conditions for the safety assessment.

3.0 VALIDATION CASE AND COMPUTATIONAL SETUP

In order to verify the applicability of the modelling approach on small-scale scenarios, DDT experiments in the GraVent facility are simulated. The GraVent test rig is a 6 m long channel with a rectangular cross section of 300 mm in width and 60 mm in height. The first 3.95 m are obstructed with obstacles blocking 60 % of the cross-section area. The obstacles are spaced with 300 mm between each other. The first obstacle is placed 50 mm behind the ignition source at the centre of one end plate. The obstacles reach across the entire width of the channel and extend from top and bottom towards the middle of the channel, respectively. The rear 2.05 m long section is unobstructed and does allow the formation of stable detonations unaffected by reflected or scattered pressure waves from the obstructed section [1].

The GraVent test rig geometry is depicted by a mesh of around about 150000 cells. The average cell size of the mesh is 8.5 mm. In the simulation a single-staged AMR is applied. Comparison of a single-staged and two-staged AMR showed similar run-up distances for the characteristic speed of sound of the combustion products. The choice of a single-staged AMR is a compromise between mesh resolution and computational time. Typical computation times of one simulation are at about 8 hours.

Due to the assumption of a homogeneous fuel, the H_2-CO-air gas mixture is initialized by the means of an unburned fuel mass fraction and a constant mass fraction of hydrogen in the fuel. The confining boundaries are all defined as adiabatic walls with no slip condition. The turbulent quantities are initialised at a very low level, because stationary conditions are assumed at the start. The ignition is realized by patching a hemisphere with a radius of 15 mm at the ignition source as fully burned gas.

4.0 RESULTS

At first the impact of the altered treatment of the critical velocity gradient in the quenching term of the TFC model is discussed. Figure 4 presents a comparison of experimental and computed flame tip velocities as a function of the leading flame tip position in the channel of the GraVent facility. The fuel content is 22.5 vol-% of pure H_2 (left) and 75/25 vol-% H_2/CO (right) as fuel. Simulations are run with g_{cr} evaluated from the correlation based on 1D simulations (solid line) and from the dimensional term in equation 5 (dash-dotted line). The horizontal dashed lines in the plots correspond to the two characteristic velocities specific for each H_2-CO-air mixture, speed of sound of combustion products a_{pr} and the Chapman-Jouguet velocity D_{CJ}. The latter is the propagation speed of a stable detonation. Only the first meters are presented in figure 4 to focus on the flame acceleration driven by the deflagration.

The velocity profiles start to deviate after the first bump, which corresponds to the second obstacle. Due to the increased velocities, strong production of turbulent kinetic energy behind the obstacle leads to partial quenching of the flame. The velocity profiles of the new correlation follow the experimental data very closely for both fuel compositions. In the case of pure H_2 fuel, the smaller critical value of g_{cr} from the dimensional term results in a stalled onset of detonation, even though a_{pr} is reached at roughly the same position. This might be due to a less intense preconditioning of the fresh gas and a belated self-ignition. As expected from the behaviour of g_{cr} on CO addition in figure 2, the impact of the quenching model is more pronounced for the fuel composition of 75 vol-% H_2. The newly presented correlation shows close agreement with the measurements, while the dimensional term for g_{cr} results in a much later onset of detonation. Thus, the proper treatment of the TFC model's quenching limits appears to be a relevant feature for the FA and DDT prediction with CO addition in small-scale obstructed channels.

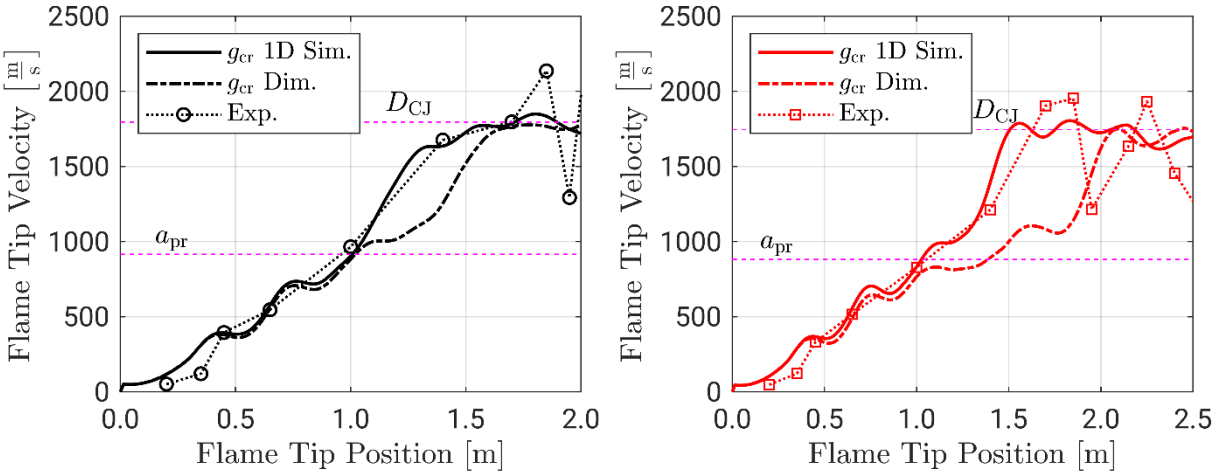

Figure 4. Flame tip velocity in the GraVent facility of 22.5 vol-% fuel in air with 100 vol-% (left) and 75 vol-% (right) H_2 in the fuel

The general importance of the correct treatment is further discussed on a comparison of computed and measured flame tip velocities in the FZK-7.2m facility [2]. The test rig is a 7.2 m long quadratic tube with circumferential obstacles inside. It has a smaller blockage ratio of 30 % and a smaller obstacle spacing of 100 m in comparison to the GraVent test rig. The experiment of interest is conducted with 15 vol-% H_2 in air. The computation is carried out on a mesh with 130000 cells and a two-staged AMR.

Due to the limited validity of the flame speed correlation and the presented g_{cr} correlation, Ettner's flame speed correlation for H_2-air mixtures is applied [6]. The computational setup is equivalent to the GraVent cases.

In figure 5 computations with neglected quenching (solid line) and the dimensional expression of equation 5 (dash-dotted line) are compared to measurement data (markers). To single out the effect of quenching on the deflagration, only the deflagrative source term is active in equation 1 for both simulations. Thus, the maximum stable flame tip velocity is the speed of sound of combustion products a_{pr} for the fast flame with neglected quenching. Like the results in the GraVent facility, the two computed profiles only start to deviate once a high enough flame velocity is reached. But the deviation is much more pronounced due to the smaller spacing of the obstacles. This can be explained by the fact, that flame quenching is dominant in the shear layer of high turbulent production behind obstacles. If the critical velocity gradient is not treated correctly according to the mixture's properties, the small g_{cr} values result in flame quenching for large portions of the fresh gas pocket behind an obstacle. This limits the growth of flame surface and thus, the acceleration of the flame. In geometries with larger spacing, a smaller portion of the fresh gas pocket behind an obstacle is cut off from the flame by quenching. This still allows for a sufficient flame surface growth in order to reach a_{pr} and eventually transition into a detonation, if the dimensional term of equation 5 is used in the GraVent simulations. The limited importance of Quenching on the prediction of correct flame velocities in large-scale scenarios can be justified likewise. But quenching cannot be omitted entirely in the TFC model, because it will occur eventually if the turbulent mixing is intense enough.

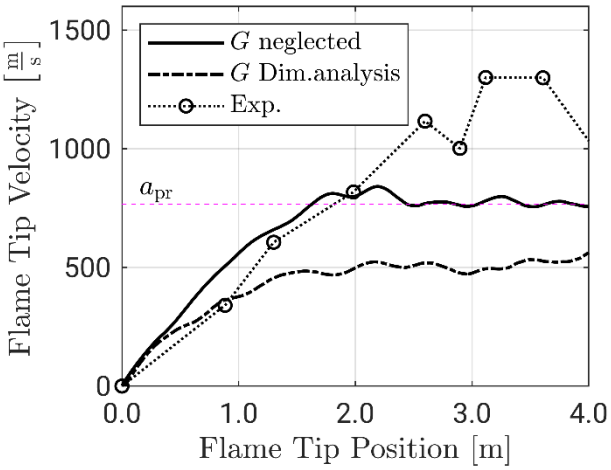

Figure 5. Flame tip velocity in the FZK-7.2m facility of 15 vol-% H_2 in air

In the following, the capability of the solver to compute FA and DDT within one framework for H_2-CO-air mixtures is verified by measurement data of the GraVent facility. In figure 6 computations (solid lines) are compared with experimental results (markers) of 22.5 vol-% (left) and 25.0 vol-% (right) fuel content with 75 vol-% H_2 in the fuel. It should be mentioned that the experimental fuel contents can show small deviations from the desired fuel content due to the complexity of the fuel injection process. The vertical dash-dotted line separates the obstructed (obs.) from the unobstructed (unobs.) section of the channel at 3.95 m.

The flame velocity profiles match the data very well for both fuel contents in figure 6. At 25 vol-% fuel D_{CJ} is reached slightly earlier by the simulation. The velocity fluctuations in the obstructed section observed in the experimental data can also be seen in the numerical results, but to a smaller extend. The fluctuations occur due to the interaction of the shock front with the obstacles reflecting and scattering waves. It should be noted, that the small amount of discrete measurement points in the experiment might contribute to the stronger fluctuations of the measured flame tip velocity. Both, experiment and numerics, display a small mean velocity deficit compared to D_{CJ} in the obstructed section of the channel.

This is in accordance to the finding for H_2-air mixtures in literature [25]. The mean velocity deficit appears to be larger in the experimental results compared to the calculations.

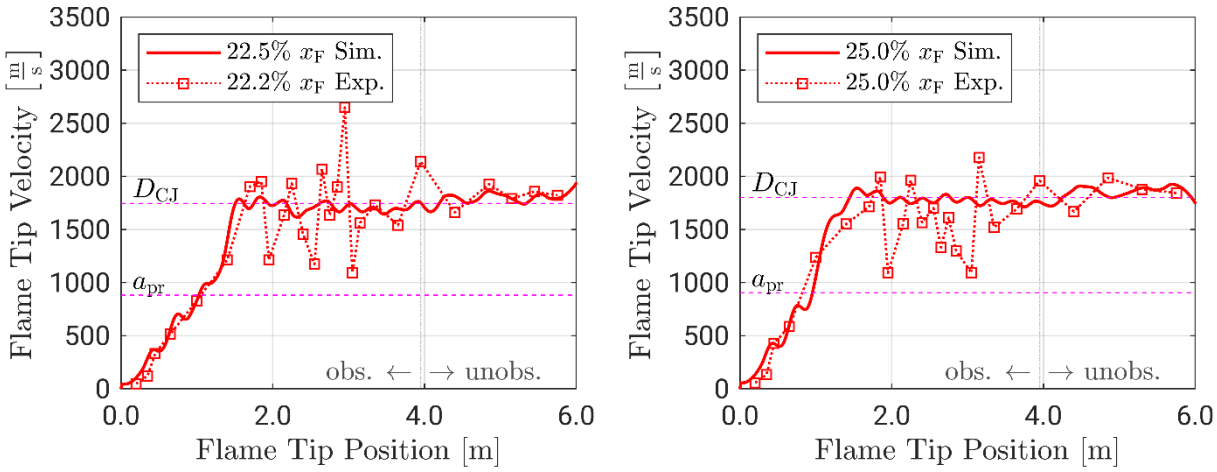

Figure 6. Validation of the numerical approach against experimental data for fuel contents of 22.5 vol-% (left) and 25.0 vol-% (right) with $x_{H2,F} = 0.75$ in the GraVent facility

When the detonation front reaches the unobstructed section after 3.95 m, the velocity rises and overshoots D_{CJ}. This corresponds to a short over compressed detonation before the velocity declines towards D_{CJ} when the flame comes close to the back plate of the channel. Overall, the good agreement in figure 6 validates the numerical approach for a small-scale application with 75 vol-% H_2 in the fuel.

The numerical approach is further checked against experiments with fuel compositions of 50/50 vol-% H_2/CO. The comparison is presented in figure 7 with fuel contents of 22.5 vol-% (left) and 25.0 vol-% (right). Again, the characteristic velocities a_{pr} and D_{CJ} are included in the plots as horizontal dashed lines. The computational results deviate from the measurements for both fuel contents. The calculated velocity profiles cross the line of a_{pr} leading to DDT. After DDT, they show comparable behaviour to the results at 75 vol-% H_2 in fuel with a small velocity deficit in the obstructed section and increased velocity in the unobstructed section. In comparison, the experimental results do not cross the velocity of a_{pr} right away.

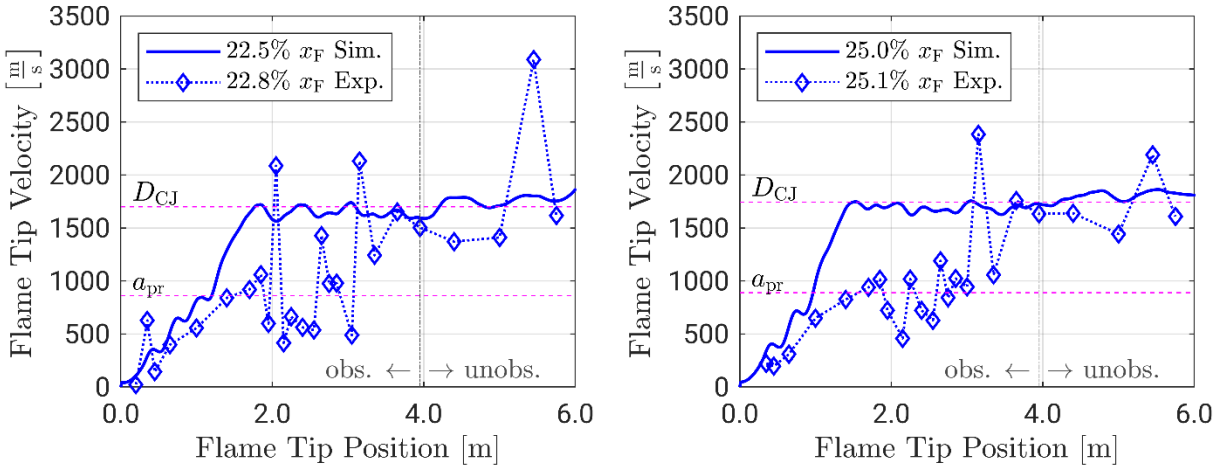

Figure 7. Validation of the numerical approach against experimental data for fuel contents of $x_F = 0.225$ (left) and $x_F = 0.250$ (right) with $x_{H2,F} = 0.50$ in the GraVent facility

The flame becomes a fast flame and, apart from some fluctuations connected to local self-ignition processes, remains around the corresponding velocity of a_{pr}. Only in the rear part of the obstructed section the flame transitions into a detonation.

The numerical approach is not capable to reproduce the measured behaviour. The reason can be traced back to the source terms of the flame propagation. The volumetric source term will be triggered whenever the pressure rises sufficiently, because the decisive ignition delay time drops drastically with the corresponding temperature increase. The characteristic pressure level for this behaviour relates to the pressure experienced after a quick acceleration to the velocity of a_{pr}. Hence, once the velocity of a_{pr} is reached, DDT is likely to occur in the simulation. The deviation of the velocity profiles during FA is caused by the occasional contribution of the volumetric source term to the acceleration process. But the mixture's reactivity is high enough for the required rapid acceleration, which results in the early DDT prediction.

In the sense of an applicable tool for safety analysis, the discussed aspects can be interpreted as a conservative treatment of the DDT phenomena, because flames that reach the speed of a_{pr} and travel into an unobstructed section will potentially transition to detonations. When the GraVent facility was opened at a later stage, it was discovered, that several obstacles have been removed from their fixing. But no clear point could be determined in the measurement campaign, when this might have occurred. This attaches an increased level of uncertainty to the measurements [1].

5.0 CONCLUSION

This study shows the capability of the presented CFD framework to predict DDT in fuel lean homogeneous H_2-CO-air mixtures in obstructed channels efficiently. In the turbulent flame speed closure model for deflagrative combustion, the aspect of partial flame quenching proved to have a significant impact on the flame acceleration and the onset of DDT in small-scale geometries. Thus, a H_2-CO-air specific correlation for the critical velocity gradient applicable to accelerating flames has been introduced. The importance of the term for the correct prediction of flame acceleration based on the TFC model appears to be even greater when the obstacle spacing decreases. As an outcome, the general applicability of the CFD solver as a safety analysis tool is extended towards small-scale scenarios with H_2-CO fuels above 20 vol-% fuel.

The advanced numerical approach has been validated against experimental flame tip velocity data of the GraVent test rig with very good agreement for fuel contents of 22.5 vol-% and 25.0 vol-% and a fuel composition of 75/25 vol-% H_2/CO. Equal to the measurements, a small velocity deficit from the speed of stable detonations D_{CJ} could be observed in the obstructed section of the channel. The validation with measurements of a fuel composition of 50/50 vol-% H_2/CO showed a distinct deviation of the measured and simulated combustion behaviour. The measured flame speed remains at the speed of sound of products before DDT occurs at the end of the obstructed section. This behaviour cannot be predicted by the numerical framework. The applied volumetric source term in the flame propagation transport equation is likely to trigger DDT, if pressure levels correspondent to a quick acceleration to a_{pr} are reached. In the sense of a safety analysis tool, this can be interpreted as a conservative treatment of DDT. To increase the general applicability of the solver, it must be validated against further obstacle configurations and differently scaled experiments in the future, but the amount of existing DDT experiments with H_2-CO-air mixtures is limited.

ACKNOWLEDGMENTS

The presented work is funded by the German Federal Ministry of Economic Affairs and Energy (BMWi) on the basis of a decision by the German Bundestag (project no 1501545A) which is gratefully acknowledged.

6.0 REFERENCES

1. Heilbronn D., Barfuss C. and Sattelmayer T., Deflagration-to-Detonation Transition of H_2-CO-Air Mixtures in an Obstructed Channel, Proceedings of the 8th International Conference on Hydrogen Safety, 24. - 26. September 2019, Adelaide, in print
2. Veser A., CO-H_2-air combustion tests in the FZK-7m-tube. Programm Nukleare Sicherheitsforschung, Jahresbericht 2001 Teil 1, Bericht FZKA-6741, 2002
3. Gauntt R., Kalinich D., Cardoni J., Phillips J., Goldmann A., Pickering S., Francis M., Robb K., Ott L., Wang D., Smith C., St.Germain S., Schwieder D. and Phelan C., Fukushima Daiichi accident study (status as of April 2012), Sandia National Laboratory Report No. SAND2012-6173, 2012
4. Lieuwen T., Yang V. and Yetter R., Synthesis gas combustion: fundamentals and applications, CRC Press, 2009, pp. 193-221.
5. Martinez-Gomez, J., Nápoles-Rivera, F., Ponce-Ortega, J. M. and El-Halwagi, M. M., Optimization of the production of syngas from shale gas with economic and safety considerations, *Applied Thermal Engineering*, 110, 678-685, 2017
6. Ettner F., Vollmer K. G. and Sattelmayer T., Numerical simulation of the deflagration-to-detonation transition in inhomogeneous mixtures, *Journal of Combustion*, 2014
7. Hasslberger J., Katzy P., Boeck L. R., and Sattelmayer, T., Computational Fluid Dynamics Simulation of Deflagration-to-Detonation Transition in a Full-Scale Konvoi-Type Pressurized Water Reactor, *Journal of Nuclear Engineering and Radiation Science*, 3(4), 2017, 041014.
8. Barfuss C., Heilbronn D. and Sattelmayer T., Numerical Simulation of Deflagration and Detonation of Homogeneous Hydrogen-Carbon Monoxide-Air Mixtures, Proceedings of the 12th International Symposium on Hazards, Prevention and Mitigation of Industrial Explosions, 12-17 August, 2018, Kansas City, USA, in print
9. Zimont V., Polifke W., Bettelini M., and Weisenstein W., An efficient computational model for premixed turbulent combustion at high Reynolds numbers based on a turbulent flame speed closure, *Journal of engineering for gas turbines and power*, 120(3), 526-532, 1998
10. Goodwin D. G., Speth R. L., Moffat H. K. and Weber B. W., Cantera: An object-oriented software toolkit for chemical kinetics, thermodynamics, and transport processes. https://www.cantera.org, Version 2.4.0., 2018
11. Menter F. R., Two-equation eddy-viscosity turbulence models for engineering applications, *AIAA journal*, 32(8), 1598-1605, 1994
12. Ciccarelli G. and Dorofeev S., Flame acceleration and transition to detonation in ducts, *Progress in Energy and Combustion Science*, *34*(4), 499-550, 2008
13. Toro E. F., Spruce M. and Speares W., Restoration of the contact surface in the HLL-Riemann solver, *Shock waves*, 4(1), 25-34, 1994
14. Hasslberger J., Numerical Simulation of Deflagration-to-Detonation Transition on Industry Scale, Dissertation, Technische Universität München, Garching, Germany, 2017
15. Li X., You X., W, F. and Law C. K., Uncertainty analysis of the kinetic model prediction for high-pressure H2/CO combustion, Proceedings of the Combustion Institute, 35(1), 617-624, 2015
16. Dinkelacker F., Manickam B. and Muppala S. P. R., Modelling and simulation of lean premixed turbulent methane/hydrogen/air flames with an effective Lewis number approach, *Combustion and Flame*, 158(9), 1742-1749, 2011
17. Davis S. G., Joshi A. V., Wang H. and Egolfopoulos F. An optimized kinetic model of H2/CO combustion, *Proceedings of the Combustion Institute*, 30(1), 1283-1292, 2005
18. Olm C., Zsély I. G., Varga T., Curran H. J. and Turányi T., Comparison of the performance of several recent syngas combustion mechanisms, *Combustion and Flame*, 162(5), 1793-1812, 2015
19. Friedrich A., Necker G., Veser A., Grune J., Kuznetsov M. and Jordan T., Experiments on the combustion behaviour of hydrogen-carbon monoxide-air mixtures, Proceedings of the 8th International Conference on Hydrogen Safety, 24. - 26. September 2019, Adelaide, in print

20. Zimont V. L., Gas premixed combustion at high turbulence. Turbulent flame closure combustion model, *Experimental thermal and fluid science*, 21(1-3), 179-186, 2000
21. Bouvet N., Halter F., Chauveau C., and Yoon Y., On the effective Lewis number formulations for lean hydrogen/hydrocarbon/air mixtures. *International journal of hydrogen energy*, 38(14), 5949-5960, 2013
22. Poinsot T. and Veynante D., Theoretical and numerical combustion. RT Edwards Inc., pp. 74-80, 2005
23. Meneveau C. and Poinsot T., Stretching and quenching of flamelets in premixed turbulent combustion, *Combustion and Flame*, 86(4), 311-332, 1991
24. Polifke W., Flohr P. and Brandt M., Modeling of inhomogeneously premixed combustion with an extended TFC model, *ASME Turbo Expo 2000: Power for Land, Sea, and Air*, American Society of Mechanical Engineers, 2000
25. Eder, A. Brennverhalten schallnaher und überschall–schneller Wasserstoff–Luft–Flammen. Dissertation, Technische Universitat München, Germany, 2001